OUKA
The University of Osaka
Institutional Knowledge Archive

Title	Fatigue life improvement of fillet welded joints by friction stir processing
Author(s)	Tang, Yongshi; Jiang, Feng; Hirohata, Mikihito et al.
Citation	Welding in the World. 2026
Version Type	VoR
URL	https://hdl.handle.net/11094/104808
rights	This article is licensed under a Creative Commons Attribution 4.0 International License.
Note	

The University of Osaka Institutional Knowledge Archive : OUKA

https://ir.library.osaka-u.ac.jp/

The University of Osaka

Welding in the World
https://doi.org/10.1007/s40194-026-02445-8

RESEARCH PAPER

Fatigue life improvement of fillet welded joints by friction stir processing

Yongshi Tang[1] · Feng Jiang[1] · Mikihito Hirohata[1] · Haruka Nakase[1] · Yoshiaki Morisada[2] · Muneaki Mukuda[2] · Hidetoshi Fujii[2]

Received: 14 July 2025 / Accepted: 29 March 2026
© The Author(s) 2026

Abstract
Friction Stir Processing (FSP) is an advanced solid-state surface treatment technique that achieves significant microstructural refinement through frictional heat generation and intense plastic deformation. This study proposes a novel methodology to enhance the fatigue performance of fillet-welded T-joints made of SM490A steel, employing Tilted Friction Stir Processing (TFSP). A total of thirteen fillet-welded specimens, fabricated using SM490A steel base metal and Z3313 T49J0T1-1CA-U weld metal, were examined, with six of them treated by TFSP. A tungsten carbide (WC) tool tilted at an angle of 9° was utilized, rotating at 600 rpm and advancing at a speed of 150 mm/min along the weld toes. Detailed microstructural analyses revealed substantial grain refinement and a 54.8% increase in Vickers hardness within the stir zone (SZ) compared to untreated regions. Four-point bending fatigue tests at a stress ratio $R = 0.1$ were performed, complemented by finite element method (FEM) analysis to elucidate stress distributions and crack initiation behaviors. Results demonstrated that TFSP significantly prolongs fatigue life, primarily due to a synergistic combination of microstructural refinement, hardness enhancement, and mitigation of stress concentration at the weld toe. Although TFSP introduced localized changes in residual stress, these had negligible adverse effects on fatigue performance. The findings underscore the efficacy of TFSP as a practical technique for fatigue improvement in welded steel structures.

Keywords Friction Stir Processing · Fatigue · Fillet-welded T-joints · Stress concentration · Microstructure refinement

1 Introduction

Steel structures, particularly steel bridges, are widely adopted due to their outstanding mechanical properties, including high strength, excellent ductility, and adaptability. Their ease of fabrication enables flexible designs suitable for various structural configurations, while their prefabrication potential considerably enhances on-site assembly efficiency. Among steel bridge components, welded joints play a pivotal role in connecting structural members, critically influencing the bridge's structural integrity and long-term reliability [1, 2]. However, fillet-welded T-joints, frequently used in frame structures, are especially susceptible to fatigue cracking under cyclic loading conditions. Fatigue cracks typically initiate at weld toes, known sites of high stress concentration, subsequently propagating and potentially leading to premature structural failures [3, 4]. Although extensive studies have focused on mitigating fatigue problems at weld toes, the persistence of fatigue-related failures highlights the urgent need for more effective treatment methods.

Several conventional post-weld treatments, including weld grinding, ultrasonic peening, hammer peening, and shot peening, have been extensively investigated for their fatigue improvement capabilities [5–10]. Weld grinding primarily reduces stress concentrations by improving weld toe geometry, effectively increasing fatigue life. However, its beneficial effects significantly diminish under high fatigue stress amplitudes, making it less reliable for critical structural components [6, 7]. Ultrasonic peening, on the other hand, modifies residual stress distribution and introduces

Recommended for publication by Commission XV - Design, Analysis, and Fabrication of Welded Structures

✉ Mikihito Hirohata
hirohata@civil.eng.osaka-u.ac.jp

[1] Graduate School of Engineering, The University of Osaka, 2-1, Yamada-osaka, Suita, Osaka 565-0871, Japan

[2] Joining and Welding Research Institute, The University of Osaka, Suita, Osaka 565-0871, Japan

Published online: 11 April 2026

beneficial compressive residual stresses at weld toes, thus enhancing fatigue resistance. Nevertheless, its effectiveness heavily depends on stringent control of process parameters, potentially limiting practical implementation due to complexity and associated quality control challenges [8–10]. These traditional approaches have thus encountered inherent trade-offs between the quality of fatigue improvement and process simplicity, underscoring the necessity for alternative solutions that combine robust fatigue enhancement with process feasibility and repeatability.

Recently, Friction Stir Processing (FSP), a solid-state surface modification technique derived from friction stir welding (FSW), has emerged as a promising approach for enhancing material fatigue properties. Originally developed by The Welding Institute (TWI) in 1991, FSW revolutionized welding technologies by enabling high-strength, defect-free joints without melting the base material [11–13]. The fundamental mechanism involves a rotating, non-consumable tool that generates frictional heat and intense plastic deformation, producing a refined, dynamically recrystallized microstructure with significantly improved mechanical properties [14–16]. This solid-state characteristic is shared by linear friction welding (LFW), which joins materials through frictional heating and intense plastic deformation without bulk melting. In contrast to fusion welding, solid-state techniques suppress solidification-related defects such as porosity, segregation, and hot cracking, while limiting the extent of the heat-affected zone and reducing thermal distortion. The combination of severe plastic deformation and dynamic recrystallization produces refined and homogeneous microstructures with improved metallurgical continuity. Studies on LFW of titanium alloys and superalloys have demonstrated that properly controlled solid-state joints can achieve mechanical properties comparable to or exceeding those of the base material, owing to grain refinement and the absence of detrimental solidification structures [17, 18]. Building on the fundamental principles of FSW, FSP was developed as a localized surface treatment method for enhancing the mechanical properties of specific structural areas without joining components. Studies have reported notable fatigue performance enhancements in various metallic alloys through microstructural refinement achieved via FSP [19, 20]. For example, Costa et al. [19] demonstrated substantial fatigue life improvements of aluminum MIG-welded T-joints by applying FSP, attributed to effective grain refinement and residual stress redistribution. Yamamoto et al. [20] similarly reported significant fatigue life extension in steel butt-welded joints after applying spherical-tip tungsten carbide tools for localized surface modification using FSP, primarily due to improved weld geometry and microstructural refinement near weld toes. Despite these advancements, the application of FSP to enhance fatigue resistance specifically in fillet-welded T-joints of steel structures remains largely unexplored. Compared to butt-welded joints, fillet welds present more complex geometrical and stress-concentration conditions, thus requiring tailored FSP strategies to effectively reduce local stress concentrations and inhibit fatigue crack initiation. Tilted Friction Stir Processing (TFSP), involving a strategically inclined tool relative to the surface normal, has recently been proposed as an effective approach for improving surface geometry and controlling flash formation, hence potentially offering substantial fatigue performance improvements [21–24]. However, the effectiveness of TFSP in enhancing fatigue life of steel fillet-welded T-joints has yet to be systematically investigated, leaving a critical research gap in understanding its applicability and mechanisms.

In this context, the present study aims to systematically evaluate the fatigue enhancement potential of TFSP applied to fillet-welded T-joints fabricated from SM490A steel. Specifically, the study investigates the effects of TFSP parameters—such as tool inclination angle, rotation speed, and travel speed—on microstructural evolution, surface geometry optimization, hardness distribution, and residual stress modification. Comprehensive four-point bending fatigue tests coupled with detailed finite element method (FEM) analyses were conducted to elucidate the relationship between local stress conditions, fatigue crack initiation behavior, and resulting fatigue life improvements. The results of this investigation not only fill a critical knowledge gap regarding TFSP's fatigue enhancement capabilities but also provide practical insights into the potential application of TFSP as a reliable fatigue countermeasure for welded steel infrastructure.

2 Experimental procedure

2.1 Materials and specimen preparation

The materials used in this investigation comprised SM490A structural steel as the base material and JIS Z3313 T49J0T1-1CA-U as the filler metal, both of which are commonly utilized in steel bridge constructions. The chemical compositions and mechanical properties of the base and filler materials are summarized in Table 1. The SM490A steel exhibits good weldability and mechanical strength, making it suitable for structural engineering applications subject to cyclic loading conditions, such as bridges and frame structures.

The T-joint specimens used in this study consisted of a skin plate measuring 300 mm in length, 200 mm in width, and 12 mm in thickness, joined to a longitudinal rib plate measuring 12 mm in height, 200 mm in length, and 12 mm in thickness as shown in Fig. 1. Prior to welding, surface contaminants such as rust, grease, and mill

Table 1 Chemical compositions and mechanical properties of base and filler materials

	Chemical compositions (%)					Mechanical properties		
	C (10^{-2})	Si (10^{-2})	Mn (10^{-2})	P (10^{-3})	S (10^{-3})	Yield stress (N/mm^2)	Tensile strength (N/mm^2)	Elongation (%)
SM490A	15	28	140	21	5	408	555	26
Z3313 T49J0T1-1CA-U	6	50	125	12	9	470	560	26

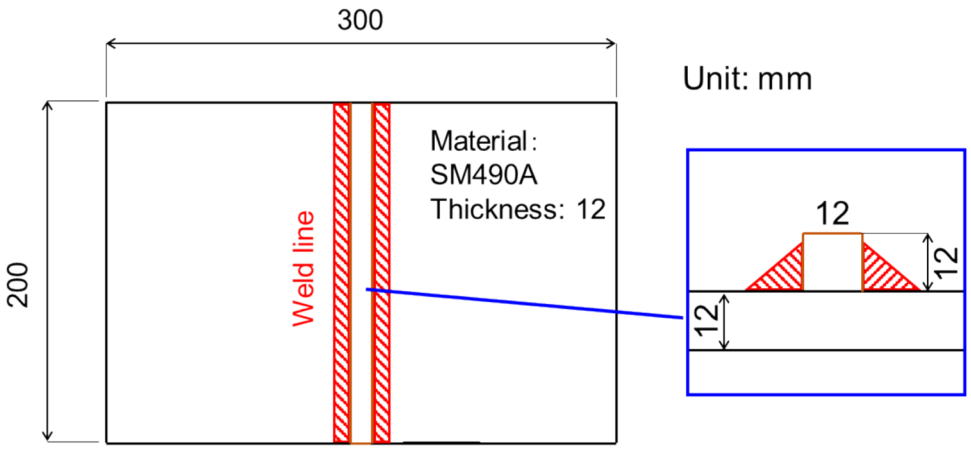


Fig. 1 Dimensions of specimens

Table 2 Welding conditions

Voltage (V)	Current (A)	Speed (mm/s)
27.6	209.6	4.2

scale were thoroughly removed by mechanical grinding and subsequent cleaning with acetone. To minimize the initial residual stresses inherent in steel fabrication, the plates were first temporarily tack-welded at the corners using spot welding and subsequently annealed at 600 °C for 2 h, followed by air cooling to room temperature.

Semi-automatic CO_2 gas-shielded arc welding (GMAW) was employed to fabricate the fillet-welded T-joints. During welding, the plates were firmly clamped onto a rigid welding table equipped with custom-designed clamps to prevent deformation and ensure consistent weld quality. The welding conditions adopted in this investigation, including voltage, current, and welding speed, are summarized in Table 2. These welding parameters were selected based on preliminary welding trials, with the goal of achieving adequate weld penetration, uniform weld bead profiles, and sufficient structural integrity typical for practical steel bridge components. Subsequently, the welded plates were cut to obtain test specimens, each 140 mm wide, by removing 30 mm from both ends of the weld bead to eliminate potential irregularities associated with weld initiation and termination regions.

Among the thirteen prepared specimens, six were designated for tilted TFSP treatment, while the remaining seven served as the control group under as-welded (AW) conditions. Prior to TFSP treatment, specimens were carefully cleaned again to remove surface oxides and contaminants, ensuring optimal conditions for subsequent surface processing.

2.2 Tilted Friction Stir Processing (TFSP) method

The TFSP employed in this study utilized a custom-designed tungsten carbide (WC) tool, carefully selected due to its high hardness, exceptional wear resistance, and suitability for processing high-strength structural steels. The tool featured a cylindrical shoulder with a diameter of 15 mm and a probe length of 7.5 mm, optimized based on preliminary trials to achieve effective stirring depth and sufficient heat generation for the SM490A steel plates employed.

To maximize the efficacy of microstructural refinement at the weld toe, the tool was strategically tilted at an angle of 9° relative to the specimen's vertical axis. The selection of a 9° tilt angle was based on prior research and preliminary testing, demonstrating improved surface finishing, controlled burr formation, and optimized material flow near the weld toes. During processing, the tool rotated at a constant speed of 600 rpm while progressing along the weld toe at a travel speed of 150 mm/min, parameters that were systematically determined from preliminary parametric

studies aimed at balancing heat input, tool wear, and effective microstructural refinement. The final parameter combination was down-selected from preliminary trials based on defined screening criteria. These criteria included minimal flash or burr formation at the weld toe, improved surface smoothness and increased toe radius, sufficient stir zone coverage of the fatigue-critical region without surface defects (e.g., grooves, undercut, or insufficient stirring), noticeable hardness enhancement compared to the as-welded condition, and stable processing behavior without excessive tool vibration or abnormal loading. The selected parameters satisfied all these requirements and ensured repeatable and defect-free processing. Each specimen was securely fixed using specially designed rigid steel fixtures, clamping both sides of the plates firmly onto a heavy-duty worktable. The robust fixture system was essential for mitigating out-of-plane deformation during TFSP and ensuring a consistent processing depth and tool trajectory. To precisely control the depth of the stir SZ, the tool shoulder was positioned to reach approximately 3.2 mm below the specimen's top surface, allowing sufficient penetration to refine microstructure effectively at critical stress-concentration zones without thinning the surface material.

In conventional FSP of butt-welded joints, positioning the retreating side (RS) of the tool at the weld toe has proven beneficial due to the natural deposition of plasticized material, filling weld toe imperfections [20]. However, preliminary tests indicated that for fillet-welded T-joints—characterized by more complex geometries—such configurations led to problematic flash (or burr) accumulation and increased local stress concentration. Hence, the advancing side (AS) of the tool, where more intensive plastic deformation and stirring occurs due to the tool's forward motion, was intentionally positioned adjacent to the weld toe. This strategic choice effectively minimized flash formation at the weld toe, ensuring smoother surface geometry and reduced stress concentrations. During processing, each side of the weld bead was treated separately. After completing TFSP on one side, the specimen was allowed to cool naturally to room temperature before processing the opposite side. This interval of controlled cooling between the two-sided processing minimized thermal distortion and residual stress gradients, resulting in more uniform microstructural refinement and balanced residual stress distributions across the weld region.

Figure 2(a) provides a schematic illustration clearly showing the TFSP tool geometry, including the dimensions and tilt angle (9°), as well as the tool's rotational direction, traveling direction, and relative positions of AS and RS. Figure 2(b) presents an actual photograph taken during TFSP processing, demonstrating the practical implementation of the setup, including the tool position and fixture system.

The selected TFSP parameters, including tilt angle, rotation speed, and travel speed, along with the strategic placement of AS near the weld toe, were comprehensively analyzed in subsequent sections to elucidate their individual and combined contributions to fatigue performance enhancement, microstructural refinement, hardness improvement, and residual stress redistribution.

2.3 Surface geometry and microstructural characterization

The surface geometry near the weld toes was quantitatively evaluated to investigate the effects of TFSP on local stress concentration factors. A laser displacement sensor system (KEYENCE, LK-G5000V; accuracy ± 0.05 mm) was utilized for high-precision measurements. Each specimen was positioned horizontally on a precision translation stage, and the laser sensor scanned across the joint region perpendicular to the weld direction at a controlled speed of 30 mm/s, with measurement intervals of 0.1 mm to capture micro-geometrical features such as burrs, flash, and

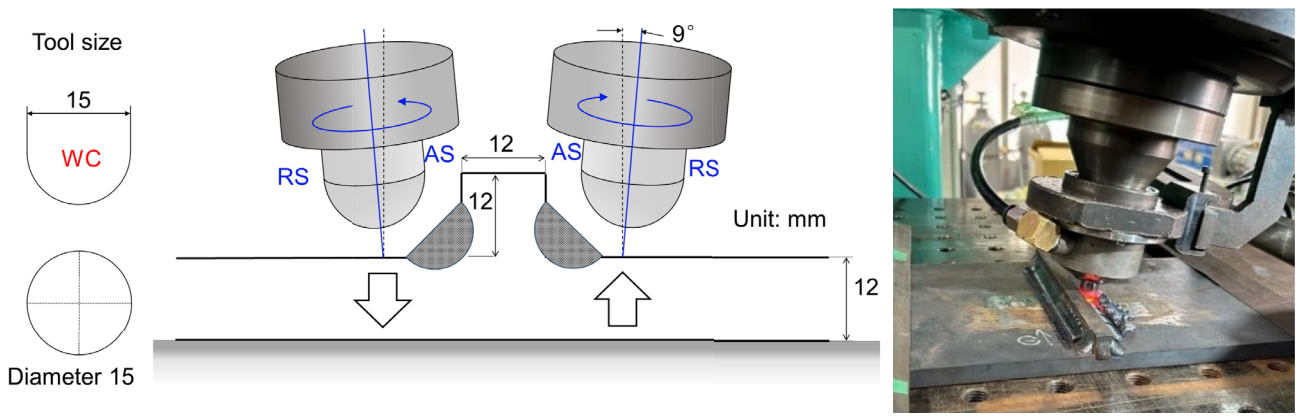


Fig. 2 Schematic diagrams of FSP: (**a**) setting and parameters of FSP; (**b**) on-site processing work

surface irregularities. Key geometric parameters, particularly the weld toe radius, were extracted from the recorded profile data and compared between TFSP-treated and as-welded (AW) specimens to evaluate the effectiveness of TFSP in reducing stress concentrations.

For microstructural characterization, cross-sectional samples were extracted from both TFSP-treated and AW specimens. Specimens were cut perpendicular to the weld line, embedded in epoxy resin, ground with silicon carbide papers, polished with diamond suspensions, and etched with 2% nital solution to reveal microstructural features. Optical microscopy (100 × –400 ×) was then performed to examine distinct zones, including the weld metal (WM), heat-affected zone (HAZ), base metal (BM), stir zone (SZ), and the SZ-HAZ transition region (SZ/HAZ interface), with particular focus on grain refinement, phase distribution, and the microstructural transition across the processed boundary. These observations provided essential insights into the microstructural mechanisms contributing to the observed enhancements in hardness and fatigue resistance following TFSP treatment.

2.4 Vickers hardness measurement

To quantitatively evaluate the effects of TFSP-induced microstructural refinement on local mechanical properties around the weld toes, Vickers hardness measurements were systematically conducted on cross-sectional specimens prepared previously for microstructural characterization, ensuring consistency between microstructural observations and mechanical evaluations. A micro-Vickers hardness tester (MICROHARDNESS TESTER FM series) was employed for measurements along horizontal lines positioned precisely at a depth of 1 mm beneath the top surface, chosen to capture hardness values from regions significantly affected by TFSP while avoiding surface roughness influences.

Vickers hardness tests were carried out under a constant load of 0.98 N (100 gf) with a dwell time of 15 s per indentation, complying with ASTM E384 standard guidelines. Indentations were spaced at 0.2 mm intervals along the measurement line, covering the region of interest from BM through HAZ, WM, SZ-HAZ transition region, and finally the SZ. Each indentation was examined microscopically to verify the absence of visible cracks or irregularities. Multiple indentation lines were performed for each specimen type (AW and TFSP-treated), and hardness values were statistically averaged at each corresponding position. The resulting hardness distributions were plotted against spatial positions to illustrate and quantify the effects of TFSP on local mechanical properties.

2.5 Residual stress measurement

To evaluate the effects of TFSP on residual stress distributions near weld toes, measurements were performed using a portable X-ray diffraction (XRD)-based residual stress analyzer (μ-X360s, Pulstec Industrial Co., Ltd.). The analyzer operates based on the cosα method, irradiating the specimen surface with a collimated Cr-Kα X-ray beam at an incident angle of approximately 35°. Residual stresses were determined by analyzing shifts in diffraction peak positions obtained from a high-sensitivity two-dimensional detector.

Measurements were systematically conducted on both as-welded (AW) and TFSP-treated specimens along transverse lines at 5 mm intervals, covering regions from 15 to 40 mm away from the weld centerline on each side. At each location, both transverse and longitudinal residual stresses were independently recorded. Prior to measurements, specimen surfaces were cleaned and gently polished to minimize surface roughness effects. Reference stress-free samples were used for calibration. Mean values and standard deviations were calculated for each measurement point, and the resulting stress distributions were analyzed to identify TFSP-induced alterations relative to the AW condition.

2.6 Fatigue experiment procedure

To evaluate the effectiveness of TFSP in enhancing the fatigue life of fillet-welded T-joints, four-point bending fatigue experiments were systematically conducted on both TFSP-treated and as-welded (AW) specimens. The four-point bending configuration was selected because it provides a constant bending moment region along the weld line, where fatigue cracks typically initiate. Each specimen had a width of 140 mm and was extracted from the original welded plates to ensure geometric consistency. To monitor local deformation and detect crack onset, strain gauges (5 mm gauge length) were attached near the weld toes on the tension side, with positions determined based on preliminary finite element analysis.

Fatigue experiments were performed on a servo-hydraulic testing machine under load control using a constant-amplitude sinusoidal waveform with a stress ratio of $R = 0.1$ and a frequency of 5 Hz. The applied load ranges were selected to generate nominal stress ranges of 210, 225, 240, 255, and 270 MPa, covering both high-cycle and medium-cycle fatigue regimes relevant to structural applications. The nominal stress was calculated from the applied load using the classical beam bending relationship for four-point bending, assuming linear elastic behavior. The load-stress conversion was further verified through finite element analysis to ensure consistency between analytical estimation and local stress distribution along the weld line. The corresponding applied

Table 3 Fatigue life of specimens with nominal stress, load range and maximum local stress

No	Nominal stress (N/mm^2)	Load range (kN)	Maximum local stress (N/mm^2)	Fatigue life (cycles)
FSP1	240	23.04	245.0	>2,592,000
FSP2	210	20.16	222.7	>2,592,000
FSP3	225	21.60	254.5	>2,592,000
FSP4	255	24.48	264.3	1,671,700
FSP5	240	23.04	298.0	899,123
FSP6	270	25.92	363.1	162,128
FSP7	255	24.48	285.8	>2,592,000
FSP8	270	25.92	275.6	>2,592,000
W1	210	20.16	249.7	>2,592,000
W2	225	21.60	262.6	1,150,895
W3	225	21.60	244.5	1,773,842
W4	240	23.04	273.3	900,000
W5	255	24.48	303.8	936,000
W6	270	25.92	318.3	88,410
W7	270	25.92	293.3	468,000

load ranges are summarized in Table 3 together with the fatigue experiment conditions for completeness.

Specimens were supported in a symmetrical four-point bending configuration with inner and outer spans of 100 mm and 240 mm, respectively (Fig. 3). Tests continued until failure or until reaching a predefined endurance limit of 2,592,000 cycles. Failure was defined by either fatigue crack detection via periodic magnetic particle inspection or a reduction in strain gauge signal amplitude of at least 5% from its stabilized cyclic value. Post-test visual and magnetic particle inspections were conducted to confirm crack initiation locations and propagation paths.

2.7 Finite Element Method (FEM) analysis

Finite Element Method (FEM) analysis was employed to investigate and quantify local stress concentrations at the weld toes of both TFSP-treated and as-welded (AW) specimens under four-point bending fatigue loading conditions. The experimentally identified fatigue crack initiation sites in Fig. 4, marked by blue circles, were used to define the

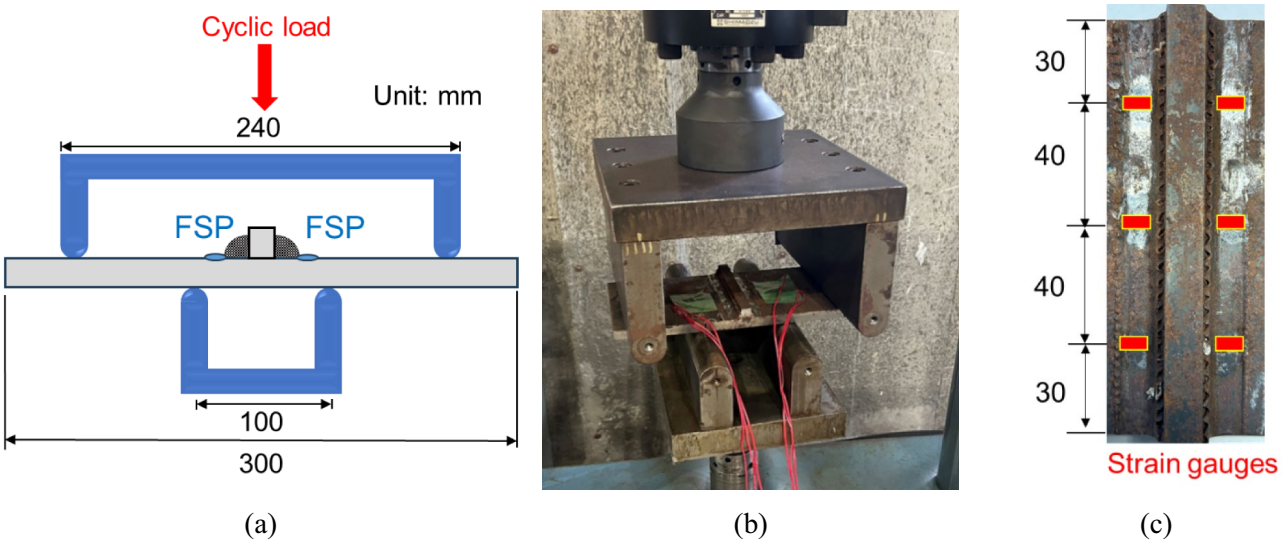


Fig. 3 Schematic diagrams of the fatigue experiment: (**a**) setup of fatigue load; (**b**) experiment situation; (**c**) strain gauge locations

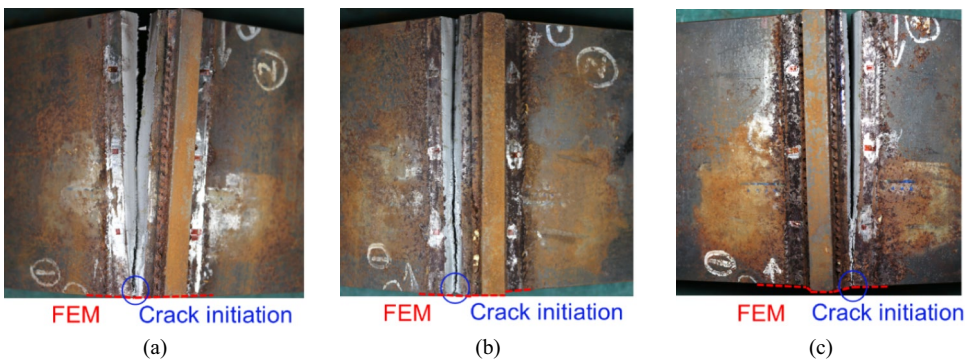


Fig. 4 Fracture surfaces of representative specimens after four-point bending fatigue failure. (**a**) Stress range of 255 N/mm^2; (**b**) stress range of 240N/mm^2; (**c**) stress range of 270N/mm.^{2}

critical regions for stress concentration evaluation. The FEM analysis was performed on the cross-sections indicated by the red lines, providing detailed insights into stress distributions and the locations of maximum local stress, which were then compared with the experimentally observed crack initiation positions. Simple two-dimensional, plane-strain elastic finite element models were constructed using the ABAQUS software (version 6.18). Model geometries accurately reflected the actual dimensions and measured weld toe geometries of experimental specimens. Material properties were assumed linear-elastic with an elastic modulus of 2.1×10^5 N/mm^2 and Poisson's ratio of 0.3, consistent with typical structural steel characteristics under low-level cyclic stresses. Boundary conditions replicated the experimental four-point bending loading configuration. Refined meshes were employed at weld toe regions to accurately capture stress gradients, while coarser meshes were used elsewhere to optimize computational efficiency.

From each FEM simulation, maximum local stresses (σ_{mloc}) at the critical weld toe locations were extracted, and stress concentration factors (K_t) were calculated using the ratio of the maximum local stress to the nominal applied stress (σ_{nom}), as defined by the relationship:

$$K_t = \frac{\sigma_{mloc}}{\sigma_{nom}} \tag{1}$$

The resulting stress concentration factors were systematically compared between TFSP-treated and AW specimens, allowing quantitative evaluation of the geometric and microstructural improvement effects introduced by TFSP. FEM results were validated by comparing stress concentration locations and magnitudes with experimentally observed fatigue crack initiation positions identified through magnetic particle inspections and visual observations.

3 Results and discussion

3.1 Effect of TFSP on surface geometry at weld toes

The surface geometry at the weld toes critically influences local stress concentrations, directly affecting fatigue performance. Figure 5 illustrates representative surface profiles measured across weld toes of the as-welded (AW) and TFSP-treated specimens, clearly highlighting the geometric modifications introduced by TFSP.

In the AW condition, the weld toe exhibited notable geometric irregularities characterized by sharp transitions and localized depressions resulting from typical fillet-welding practices. Such geometric irregularities inherently increase local stress concentrations, creating preferential initiation sites for fatigue cracking under cyclic loading conditions. After applying TFSP, substantial improvements in surface geometry were observed. As depicted in Fig. 5(b), the TFSP-treated region displayed a notably smoother and more regular surface profile adjacent to the weld toe. The strategic placement of the AS of the rotating tool near the weld toe successfully minimized flash formation and burr

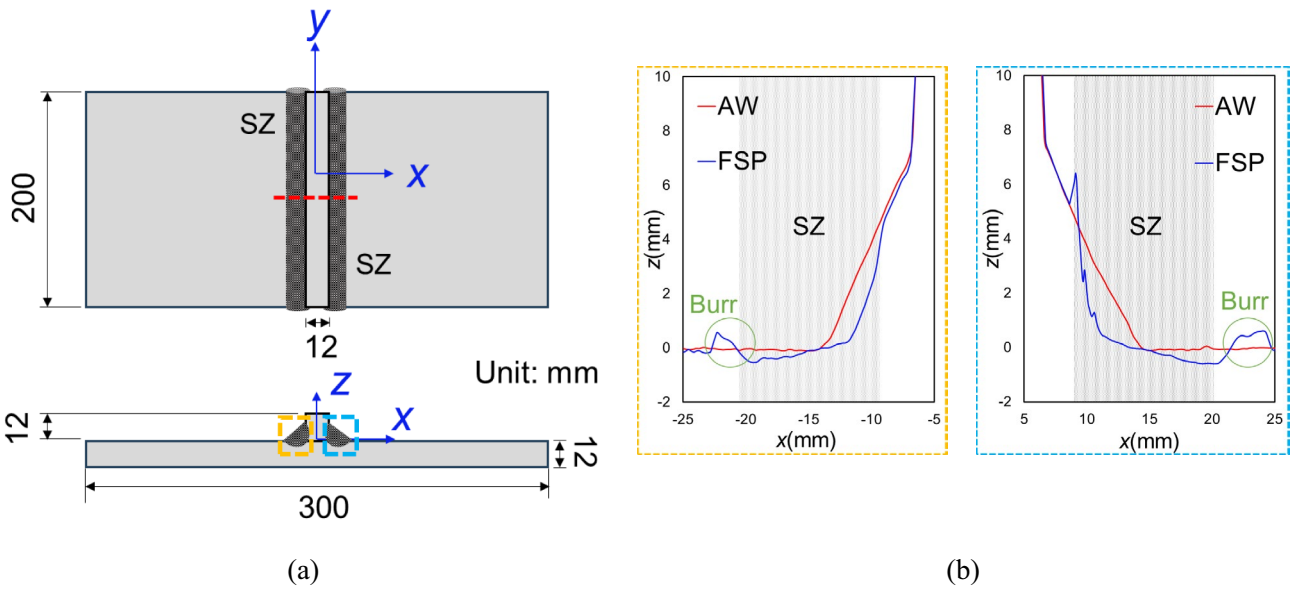


Fig. 5 Specimen size and measurement results of welded joint surface geometry: (**a**) location of the cross-section (red dotted line); (**b**) results of AW and FSP-treated specimens

accumulation, thus significantly reducing geometric discontinuities and surface roughness. Specifically, the weld toe radius was noticeably enlarged, and previously sharp transitions were effectively smoothed, directly contributing to stress concentration reductions. In contrast, a notable flash formation was observed on the RS, away from the weld toe region. This localized flash (highlighted by green circles in Fig. 5(b)) arose due to material flow characteristics associated with the tool's rotation direction and inclination angle. However, since this flash was located far from the critical weld toe regions, its impact on local fatigue resistance was considered minimal.

These observed geometric modifications at weld toes after TFSP directly correlate with subsequent reductions in local stress concentration factors, as quantitatively confirmed by FEM analyses presented in later sections (see Sect. 3.4). Consequently, the optimized weld toe geometry achieved through TFSP provides an essential foundation for improved fatigue performance in fillet-welded steel joints.

3.2 Microstructural evolution and hardness improvement

The microstructural evolution induced by TFSP treatment significantly influenced local mechanical properties at the weld toe region. Representative optical micrographs obtained from different regions across the specimen cross-section, including the weld metal (WM), heat-affected zone (HAZ), base metal (BM), stir zone (SZ), and the SZ-HAZ transition region, are illustrated clearly in Fig. 6. In the weld metal (WM) region (Fig. 6(b)), a characteristic mixed microstructure consisting of bainite and ferrite was observed, featuring coarse and elongated grain morphologies typically generated by arc welding thermal cycles. The adjacent HAZ (Fig. 6(c)) displayed a predominantly ferritic microstructure with partial bainitic transformation, indicating moderate thermal influence during welding. In contrast, the base metal (BM, Fig. 6(d)) exhibited a uniform and equiaxed ferritic grain structure, reflecting the original hot-rolled condition of the SM490A steel plate. Notably, in the TFSP-treated region (SZ, Fig. 6(e)), significant grain refinement was achieved due to intense plastic deformation and dynamic recrystallization. The SZ exhibited substantially finer, equiaxed ferritic grains compared to other regions. Furthermore, the SZ-HAZ transition region (Fig. 6(f)) exhibited partially deformed and partially recrystallized microstructures, reflecting the steep gradients of strain and temperature between the heavily stirred SZ and the purely heat-affected region. From a mechanistic perspective, the WM microstructure (Fig. 6(b)) is governed by melting/solidification during GMAW and subsequent solid-state transformations upon cooling, which typically produce relatively coarse, heterogeneous ferrite/bainite morphologies. The HAZ (Fig. 6(c)) does not melt, but experiences a welding thermal cycle; depending on the peak temperature and cooling rate, partial or full austenitization followed by transformation during cooling results in a mixed and spatially heterogeneous microstructure compared with the BM (Fig. 6(d)). In contrast, the SZ (Fig. 6(e))

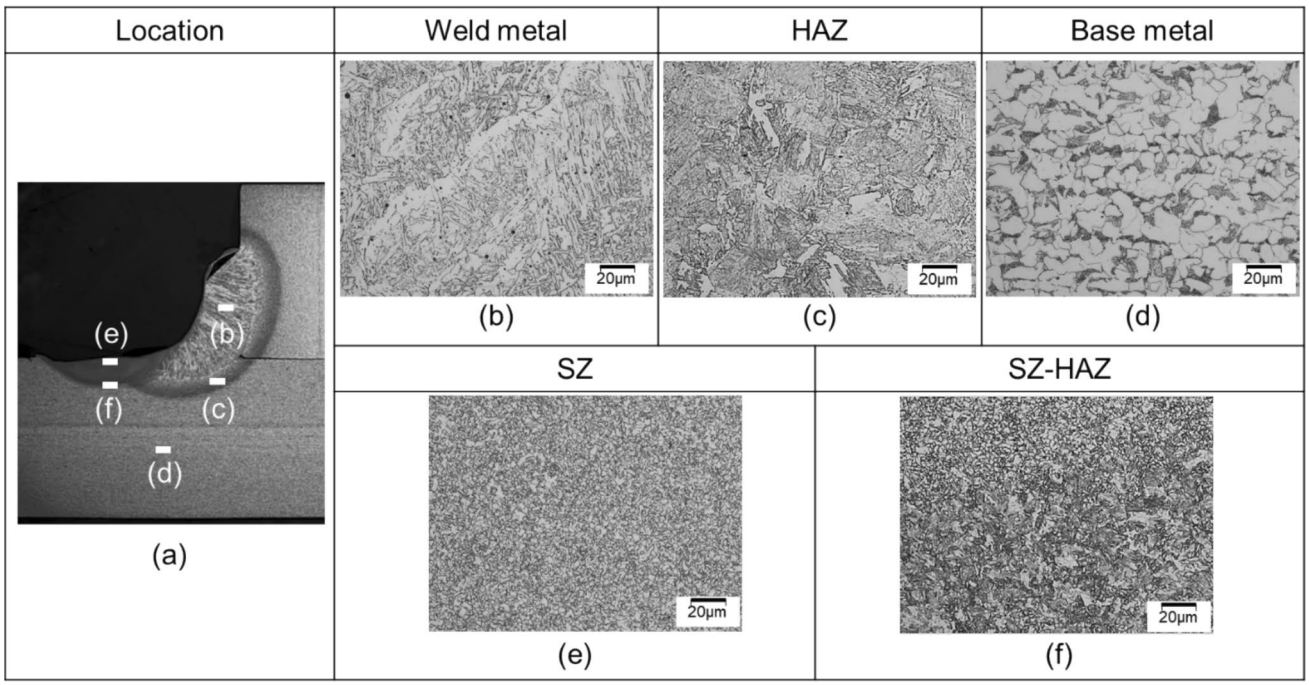


Fig. 6 Cross-sectional OM observations of (**a**) measurement locations, (**b**) weld metal, (**c**) HAZ, (**d**) base metal, (**e**) SZ, and (**f**) SZ-HAZ

undergoes intense plastic shear deformation under frictional heating during TFSP, promoting dynamic recrystallization and producing fine, equiaxed grains. Across the SZ-HAZ transition region (Fig. 6(f)), the imposed strain and temperature decrease rapidly with distance from the tool, so recrystallization becomes incomplete and a gradient microstructure forms. This gradient microstructure is consistent with the gradual hardness change from the SZ to the surrounding regions observed in Fig. 7.

The microstructural refinement and modification in the SZ significantly improved local mechanical properties, as quantitatively demonstrated by hardness measurements. Figure 7 compares the Vickers hardness distributions at a consistent depth of 1 mm below the surface across both AW and TFSP-treated specimens. The hardness profile clearly reveals distinct hardness gradients corresponding to the microstructural differences described earlier. In the AW specimen, typical hardness values for the base metal, HAZ, and weld metal were approximately 167 Hv, 204 Hv, and 217 Hv, respectively. In comparison, the SZ region in the TFSP-treated specimen displayed dramatically enhanced hardness, with an average peak value reaching approximately 336 Hv—representing an increase of about 54.8% compared to untreated areas. This substantial hardness increment is primarily attributed to TFSP-induced grain refinement and the increased dislocation density associated with severe plastic deformation in the SZ.

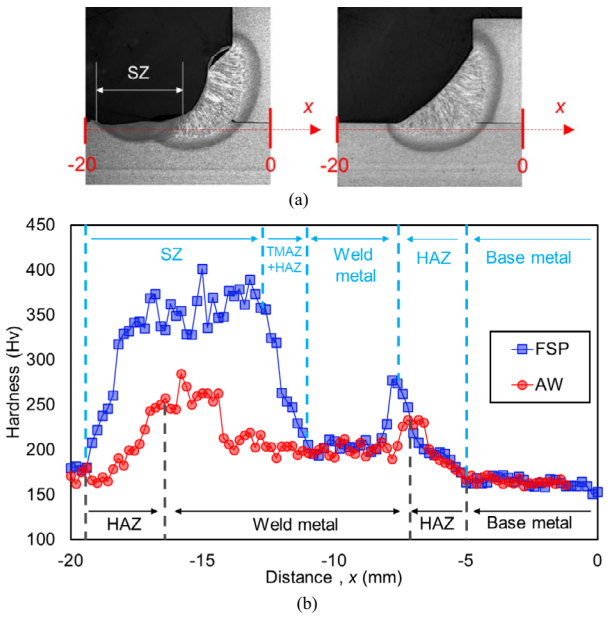


Fig. 7 OM images near the weld toe of the joints and hardness measurement results: (**a**) hardness measurement locations of AW and FSP; (**b**) Vickers hardness variation with distance from the SZ measured along a red line

Additionally, the hardness profile delineates a gradual transition from the SZ to the SZ-HAZ transition region and the surrounding HAZ, further supporting the gradient microstructure observed in Fig. 6. The improved hardness in the SZ contributes directly to increased fatigue resistance by enhancing local strength and delaying crack initiation at the critical weld toe regions.

3.3 Influence of TFSP on residual stress distribution

Figure 8 shows measured transverse (perpendicular to the weld direction) and longitudinal (parallel to the weld direction) residual stress distributions across both as-welded (AW) and TFSP-treated specimens. Measurement points were systematically positioned at intervals of 5 mm from 15 to 40 mm away from the weld centerline, providing comprehensive insight into residual stress modifications resulting from TFSP. As shown in Fig. 8(b), transverse residual stresses, which are critical for fatigue crack initiation and propagation at the weld toe, exhibited minimal changes after TFSP treatment compared to the AW condition. Both conditions presented moderate tensile transverse residual stresses across the measurement regions, indicating that the TFSP process did not significantly alter the transverse stress state. The slight increase observed after TFSP can be attributed to localized transverse plastic flow induced by tool rotation. However, because the processed zone is strongly constrained by the surrounding base material, stress relaxation is restricted, and the magnitude of transverse stress modification remains limited. Moreover, notable changes were observed in the longitudinal residual stress distributions (Fig. 8(c)). Specifically, TFSP introduced higher tensile residual stresses along the longitudinal direction, with measured values distinctly greater than those observed in the AW specimens. This increase is primarily associated with the additional thermomechanical cycle introduced by TFSP. During processing, intense frictional heating and severe plastic deformation occur beneath the rotating tool. Although material softening occurs at elevated temperature, subsequent cooling under significant mechanical constraint from the surrounding rigid material produces non-uniform thermal contraction. The restricted longitudinal shrinkage along the tool travel direction generates additional tensile residual stresses. Because material flow and cumulative plastic strain are predominantly aligned with the processing direction, the longitudinal stress component is more strongly affected than the transverse component.

Although TFSP increased the longitudinal residual stress level, transverse residual stress remains the dominant component governing fatigue performance under bending. In bending-dominated loading, the maximum tensile stress develops at the surface and is primarily oriented transverse to the weld toe. Therefore, transverse residual stresses

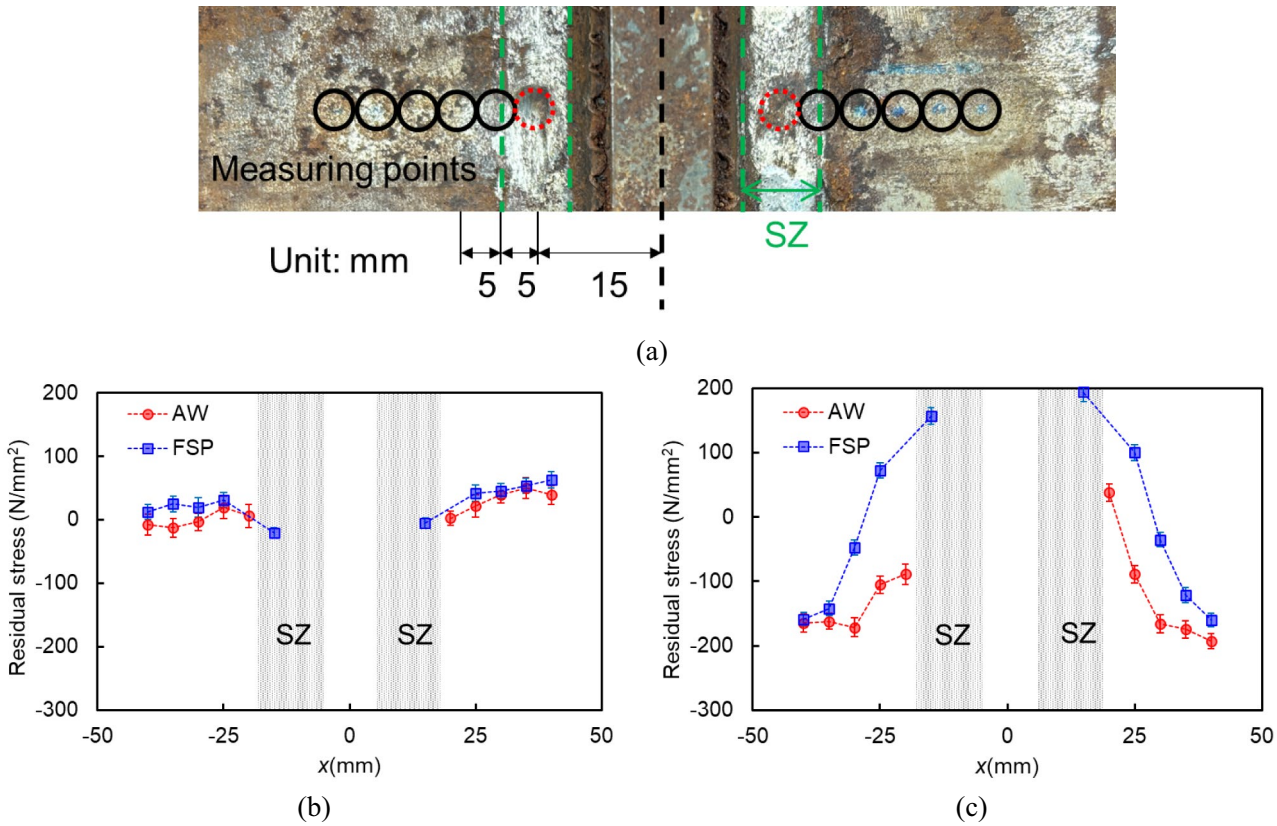


Fig. 8 Residual stress variation with distance from the weld center measured at measuring points: (**a**) surface images of the specimen with residual stress measuring points; (**b**) transverse residual stress; (**c**) longitudinal residual stress

directly superimpose onto the applied tensile stress, increasing the local maximum principal stress and crack-driving force. In contrast, longitudinal residual stresses are not collinear with the principal tensile stress under bending and thus exert comparatively limited influence on crack initiation. Consistent with this stress interaction mechanism, the increase in longitudinal residual stress did not result in measurable deterioration of fatigue life.

Overall, these residual stress measurement results indicate that the primary fatigue life improvements attributed to TFSP arise mainly from geometric smoothing, microstructural refinement, and associated hardness increases at the weld toe, rather than substantial beneficial alterations in transverse residual stresses. This observation underscores the importance of geometry and local mechanical property improvements in enhancing fatigue resistance through TFSP.

3.4 Fatigue life improvement by TFSP

To quantitatively assess the effectiveness of TFSP in enhancing fatigue resistance, four-point bending fatigue experiments were systematically conducted on both AW and TFSP-treated specimens. The corresponding fatigue test results are summarized in Table 3, while Fig. 9(a) illustrates the fatigue life performance (S–N curves) based on the applied nominal stress amplitudes. It should be noted that FSP1 and FSP7 correspond to the same specimen, and FSP3 and FSP8, W1 and W7 also correspond to identical specimens in Table 3. As clearly shown in Fig. 9(a), TFSP-treated specimens generally demonstrated substantial fatigue life improvement compared to the AW condition. Under identical nominal stress conditions, TFSP specimens exhibited significantly longer fatigue lives, with several specimens achieving the predetermined fatigue life threshold (2,592,000 cycles) without failure, effectively indicating infinite fatigue life. Specifically, at the nominal stress level of 240 N/mm^2, while AW specimens failed relatively early (around 900,000 cycles), corresponding TFSP specimens demonstrated markedly increased fatigue lives exceeding the endurance limit. Nevertheless, variability was observed among TFSP-treated specimens. For example, TFSP specimens (e.g., FSP5 and FSP6) at higher nominal stress levels ($\geq$ 255 N/mm^2) showed limited or no improvement relative to AW specimens. Subsequent FEM analyses provided further insights into this variability by considering local stress concentration effects at weld toes. Figure 9(b) presents the modified S–N curves based on maximum local stress (σ_{mloc}), calculated through FEM,

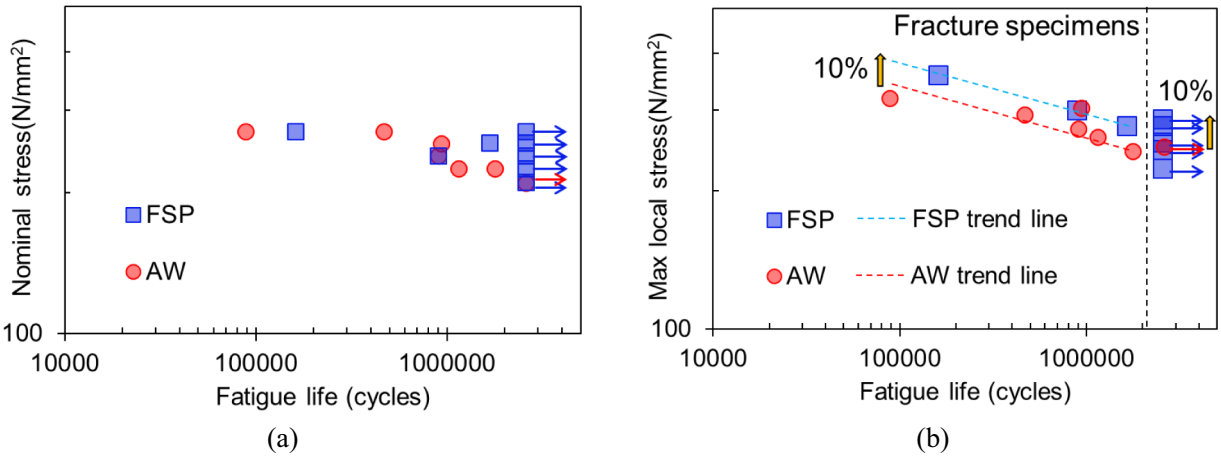


Fig. 9 S–N curves obtained from fatigue experiments: (**a**) plotted as a function of nominal stress amplitude; (**b**) replotted using the maximum local stress. The corresponding applied load ranges are provided in Table 3

to effectively decouple the influence of geometric factors from microstructural refinement. After this normalization, TFSP specimens still exhibited approximately a 10% higher fatigue limit and trend line of fracture specimens compared to AW specimens, indicating that microstructural refinement and associated hardness improvements independently contributed positively to fatigue resistance enhancement.

To further elucidate fatigue failure mechanisms, Fig. 10 presents FEM analysis results and observed fatigue crack initiation sites. For specimens FSP5 and FSP6, which showed no significant life improvement, FEM results indicated higher local stress concentration factors ($K_t \approx 1.24$) occurring near the weld toe region on the AS. In contrast, for specimens such as FSP4, which showed substantial fatigue life improvement (~ 80% increase), the FEM analysis revealed lower local stress concentration factors ($K_t \approx 1.03$) positioned slightly away from the weld toe region. Moreover, FEM analysis for non-failed TFSP specimens (Fig. 11) consistently indicated maximum stress locations on the RS away from the weld toe region, where stress concentration factors were substantially lower (average $K_t \approx 1.05$). These findings clearly illustrate that proper TFSP treatment not only improves surface geometry, significantly reducing concentrations of local stress, but also effectively shifts crack initiation sites away from critical weld toe regions, thus substantially increasing fatigue life. Conversely, partial failures observed in some TFSP specimens suggest incomplete or suboptimal TFSP processing, possibly due to variations in processing parameters or tool alignment. These variations resulted in insufficient geometry improvements and elevated local stress concentrations at critical weld toe regions, limiting fatigue life enhancement despite the refined microstructure and increased hardness.

Despite the pronounced grain refinement in the stir zone (SZ), fatigue cracks in FSP5 and FSP6 still initiated within this region, indicating that local stress concentration dominated over intrinsic microstructural strengthening. Although grain refinement and the associated hardness increase enhance resistance to crack nucleation, they cannot counteract a relatively high stress concentration factor ($K_t \approx 1.24$). Fatigue crack initiation is governed by the local maximum principal stress; once geometric discontinuities elevate this stress beyond a critical level, crack formation becomes unavoidable. Potential hardness gradients between the SZ and adjacent regions may further promote local strain incompatibility, facilitating crack nucleation. These results confirm that microstructural refinement alone is insufficient when geometric stress amplification persists.

From a mechanistic perspective, fatigue performance is controlled primarily by the local stress state rather than bulk strength. In FSP5 and FSP6, the high K_t maintained a strong crack-driving force, resulting in fatigue lives comparable to the AW condition. In contrast, FSP4 exhibited a markedly reduced stress concentration factor ($K_t \approx 1.03$), lowering the local maximum stress and allowing the microstructural strengthening to manifest as a pronounced life extension. Thus, geometric stress reduction governs fatigue improvement, while microstructural refinement provides a conditional enhancement under cyclic loading.

Collectively, the fatigue test and FEM results strongly support the conclusion that TFSP significantly enhances fatigue life in fillet-welded steel T-joints primarily through geometric smoothing, microstructural refinement, and hardness improvement. Notably, specimens with suboptimal performance despite microstructural refinement suffered from insufficient weld toe smoothing, resulting in high stress concentration (K_t). This underscores the necessity of

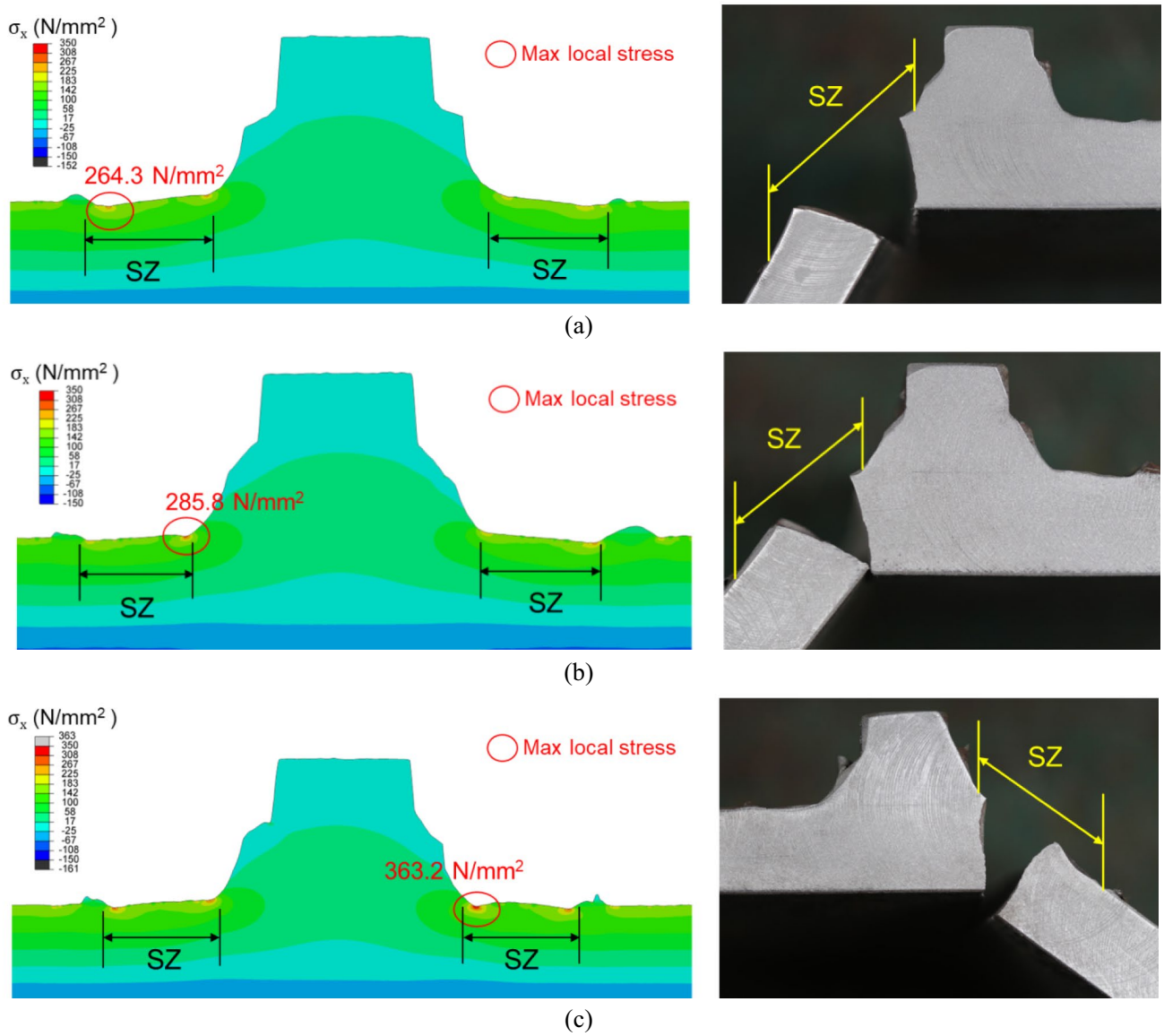


Fig. 10 FEM models for fatigue fracture FSP specimens: (**a**) FSP4; (**b**) FSP5; (**c**) FSP6

simultaneously optimizing geometry and microstructure. To achieve consistent fatigue improvement, precise control of TFSP parameters and careful monitoring of tool position relative to the weld toe are crucial.

4 Conclusions

This study systematically investigated the effectiveness of TFSP in improving the fatigue performance of fillet-welded T-joints fabricated from SM490A structural steel. Detailed experiments, including surface geometry measurements, microstructural characterization, Vickers hardness testing, residual stress measurements, and four-point bending fatigue tests, complemented by finite element method (FEM) analyses, were conducted. The main conclusions drawn from this research are as follows:

- Surface geometry improvement: TFSP significantly improved the weld toe geometry by producing smoother surfaces and enlarged weld toe radii, thereby substantially reducing geometric irregularities and local stress concentrations at weld toes. This optimized surface geometry plays a critical role in delaying fatigue crack initiation.
- Microstructural refinement and hardness enhancement: TFSP effectively induced substantial grain refinement in the SZ, resulting in the formation of fine, equiaxed

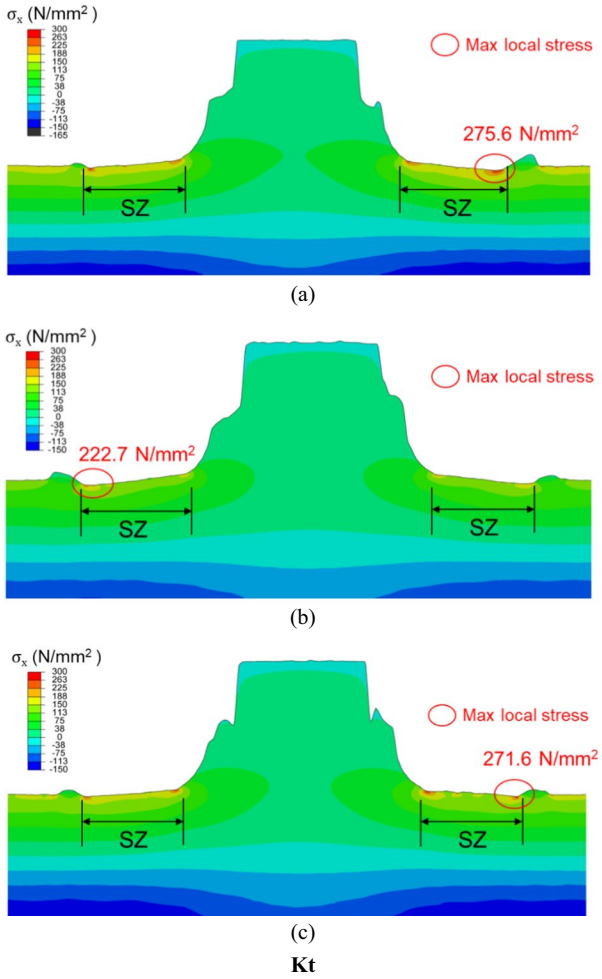


Fig. 11 FEM models for no fatigue failure FSP specimens: (**a**) FSP1; (**b**) FSP2; (**c**) FSP3

ferritic grains. Consequently, Vickers hardness values in the SZ increased significantly, reaching approximately 336 Hv, representing an approximately 54.8% increase relative to untreated weld metal regions (217 Hv). This localized strengthening contributes directly to enhanced fatigue resistance.

- Residual stress influence: Although TFSP treatment introduced increased longitudinal residual stresses due to severe plastic deformation and thermal effects, minimal changes were observed in transverse residual stresses, which are more critical for fatigue crack initiation. Thus, fatigue performance improvements were predominantly attributed to geometric and microstructural enhancements rather than significant modifications of transverse residual stresses.
- Fatigue life improvement: Four-point bending fatigue experiments clearly demonstrated that TFSP significantly increased fatigue life compared to untreated (as-welded, AW) specimens, with fatigue life improvements exceeding 100% in several cases. FEM analysis further confirmed that the fatigue life enhancement primarily resulted from reduced local stress concentration at weld toes and microstructural strengthening, as evidenced by reduced stress concentration factors (K_t) and shifted crack initiation sites away from critical weld toe regions.
- Critical factors for consistent fatigue improvement: The suboptimal performance of certain specimens arises from insufficient geometric improvement at the weld toe (higher K_t), despite microstructural refinement. This highlighted the importance of precisely controlled TFSP parameters and tool positioning. Inconsistent processing can result in inadequate geometric and microstructural improvements, limiting fatigue enhancement effectiveness.

Overall, this study demonstrates the potential of TFSP as a practical and highly effective fatigue life enhancement technique for fillet-welded T-joints in steel structures. Future research should focus on further optimization of TFSP parameters, development of robust processing guidelines, and investigation of TFSP's applicability in fatigue crack repair scenarios to extend structural life and integrity.

Author contribution Conceptualization: M. Hirohata and H. Fujii. Methodology: M. Hirohata, H. Fujii, Y. Morisada, M. Mukuda. Investigation: Y. Tang, F. Jiang, H. Nakase. Writing—Original Draft: Y. Tang, H. Nakase. Writing—Review & Editing: M. Hirohata, F. Jiang. Supervision: M. Hirohata, H. Fujii.

Funding Open Access funding provided by The University of Osaka. Part of this study was conducted with the support of JSPS KAKENHI Grant Number 23K22847.

Declarations

Competing interests The authors declare no competing interests.

Open Access This article is licensed under a Creative Commons Attribution 4.0 International License, which permits use, sharing, adaptation, distribution and reproduction in any medium or format, as long as you give appropriate credit to the original author(s) and the source, provide a link to the Creative Commons licence, and indicate if changes were made. The images or other third party material in this article are included in the article's Creative Commons licence, unless indicated otherwise in a credit line to the material. If material is not included in the article's Creative Commons licence and your intended use is not permitted by statutory regulation or exceeds the permitted use, you will need to obtain permission directly from the copyright holder. To view a copy of this licence, visit http://creativecommons.org/licenses/by/4.0/.

References

1. Soroushian P, Choi KB (1987) Steel mechanical properties at different strain rates. J Struct Eng 113(4):663–672.https://doi.org/10.1061/(ASCE)0733-9445(1987)113:4(663)
2. Da Silva AL, Correia JA, De Jesus AM, Lesiuk G, Fernandes AA, Calçada R, Berto F (2019) Influence of fillet end geometry on fatigue behaviour of welded joints. Int J Fatigue 123:196–212.https://doi.org/10.1016/j.ijfatigue.2019.02.025
3. Tovo R, Lazzarin P (1999) Relationships between local and structural stress in the evaluation of the weld toe stress distribution. Int J Fatigue 21(10):1063–1078. https://doi.org/10.1016/S0142-1123(99)00089-4
4. Ngoula DT, Beier HT, Vormwald M (2017) Fatigue crack growth in cruciform welded joints: influence of residual stresses and of the weld toe geometry. Int J Fatigue 101:253–262. https://doi.org/10.1016/j.ijfatigue.2016.09.020
5. Gao W, Wang D, Cheng F, Deng C, Liu Y, Xu W (2015) Enhancement of the fatigue strength of underwater wet welds by grinding and ultrasonic impact treatment. J Mater Process Technol 223:305–312. https://doi.org/10.1016/j.jmatprotec.2015.04.013
6. Hansen AV, Agerskov H, Bjørnbak-Hansen J (2007) Improvement of fatigue life of welded structural components by grinding. Weld World 51:61–67. https://doi.org/10.1007/BF03266561
7. Braun M, Baumgartner J, Hofmann G, Drebenstedt K, Bauer NM, Bakhschi H, Kuhlmann U (2023) A statistical assessment of the fatigue strength improvement of butt-welded joints by flush grinding. Weld World 67(10):2345–2359. https://doi.org/10.1007/s40194-023-01569-5
8. Zhao X, Wang M, Zhang Z, Liu Y (2016) The effect of ultrasonic peening treatment on fatigue performance of welded joints. Materials 9(6):471. https://doi.org/10.3390/ma9060471
9. Lago J, Trško L, Jambor M, Nový F, Bokůvka O, Mičian M, Pastorek F (2019) Fatigue life improvement of the high strength steel welded joints by ultrasonic impact peening. Metals 9(6):619. https://doi.org/10.3390/met9060619
10. Malaki M, Ding H (2015) A review of ultrasonic peening treatment. Mater Des 87:1072–1086. https://doi.org/10.1016/j.matdes.2015.08.102
11. Mirzadeh H (2021) High strain rate superplasticity via friction stir processing (FSP): a review. Mater Sci Eng A 819:141499. https://doi.org/10.1016/j.msea.2021.141499
12. Ma Z (2008) Friction stir processing technology: a review. Metall Mater Trans A Phys Metall Mater Sci 39(3):642–658. https://doi.org/10.1007/s11661-007-9459-0
13. Fujii H (2011) Friction stir welding of steels. Weld Int 25(04):260–273. https://doi.org/10.1080/09507111003655358
14. Chen YC, Fujii H, Tsumura T, Kitagawa Y, Nakata K, Ikeuchi K, Matsubayashi K, Michishita Y, Fujiya Y, Katoh J (2009) Friction stir processing of 316L stainless steel plate. Sci Technol Weld Join 14(3):197–201. https://doi.org/10.1179/136217108X386527
15. Fujii H, Cui L, Tsuji N, Maeda M, Nakata K, Nogi K (2006) Friction stir welding of carbon steels. Mater Sci Eng A 429(1–2):50–57. https://doi.org/10.1016/j.msea.2006.04.118
16. Murr LE (2010) A review of FSW research on dissimilar metal and alloy systems. J Mater Eng Perform 19:1071–1089. https://doi.org/10.1007/s11665-010-9598-0
17. Dang M, Guo Z, Ma T, Yang X, Su Y, Li W, Li J, Vairis A (2025) Microstructure evolution and mechanical properties of a linear friction welded TC4-DT titanium alloy joint. Mater Today Commun 46:112684. https://doi.org/10.1016/j.mtcomm.2025.112684
18. Yu SU, Xiawei YANG, Tingxi MENG, Dong WU, Rui XU, Haiyu XU, Su Y, Yang X, Meng T, Wu D, Xu R, Xu H, Li W, Yin S, Shuo YIN (2024) Effect of linear friction welding process on microstructure evolution, mechanical properties and corrosion behavior of GH4169 superalloy. Chin J Aeronaut 37(6):504–520. https://doi.org/10.1016/j.cja.2024.03.039
19. Costa JDM, Jesus JS, Loureiro A, Ferreira JAM, Borrego LP (2014) Fatigue life improvement of mig welded aluminium T-joints by friction stir processing. Int J Fatigue 61:244–254. https://doi.org/10.1016/j.ijfatigue.2013.11.004
20. Yamamoto H, Danno Y, Ito K, Mikami Y, Fujii H (2018) Weld toe modification using spherical-tip WC tool FSP in fatigue strength improvement of high-strength low-alloy steel joints. Mater Des 160:1019–1028. https://doi.org/10.1016/j.matdes.2018.10.036
21. Molla Ramezani N, Davoodi B (2024) Evaluating the influence of various friction stir processing strategies on surface integrity of hybrid nanocomposite Al6061. Sci Rep 14(1):8056. https://doi.org/10.1038/s41598-024-58714-3
22. Ambrosio D, Sharma A, Mukuda M, Morisada Y, Fujii H (2024) Feasibility of friction stir welding using a hemispherical tool tilted towards the retreating side. J Adv Join Process 9:100180. https://doi.org/10.1016/j.jajp.2023.100180
23. Mukuda M, Noguchi A, Morisada Y, Fujii H (2024) Development of friction stir welding method using a tilted spherical tool. Sci Technol Weld Join. https://doi.org/10.1177/13621718241231389
24. Moreira PMGP, De Figueiredo MAV, De Castro PMST (2007) Fatigue behaviour of FSW and MIG weldments for two aluminium alloys. Theor Appl Fract Mech 48(2):169–177. https://doi.org/10.1016/j.tafmec.2007.06.001

Publisher's Note Springer Nature remains neutral with regard to jurisdictional claims in published maps and institutional affiliations.